IC/2002/63

United Nations Educational Scientific and Cultural Organization
and
International Atomic Energy Agency

THE ABDUS SALAM INTERNATIONAL CENTRE FOR THEORETICAL PHYSICS

SEISMIC MICROZONING OF SANTIAGO DE CUBA: AN APPROACH BY SH WAVES MODELLING

Leonardo Alvarez*
Centro Nacional de Investigaciones Sismológicas (CENAIS), Cuba
and
The Abdus Salam International Centre for Theoretical Physics (ICTP), Trieste, Italy,

Julio García
Centro Nacional de Investigaciones Sismológicas (CENAIS), Cuba,

Franco Vaccari
Istituto Nazionale di Geofisica e Vulcanologia, Osservatorio Vesuviano (INGV-OV) Naples, Italy
and
Dipartimento di Scienze della Terra, Università di Trieste (DST), Trieste, Italy

Giuliano F. Panza
Dipartimento di Scienze della Terra, Università di Trieste (DST), Trieste, Italy
and
The Abdus Salam International Centre for Theoretical Physics (ICTP), Trieste, Italy,

Bertha González, Carmen Reyes, Bárbara Fernández,
Centro Nacional de Investigaciones Sismológicas (CENAIS), Cuba,

Ramón Pico
Instituto de Cibernética, Matemática y Física (ICIMAF), Cuba,

José A. Zapata and Enrique Arango
Centro Nacional de Investigaciones Sismológicas (CENAIS), Cuba.

MIRAMARE - TRIESTE
July 2002

* Regular Associate of the Abdus Salam ICTP.

Abstract

The expected ground motion in Santiago de Cuba basin from earthquakes which occurred in the Oriente fault zone is studied. Synthetic SH-waves seismograms have been calculated along four profiles in the basin by the hybrid approach (modal summation for the path source-profile and finite differences for the profile) for a maximum frequency of 1 Hz. The response spectra ratio (RSR) has been determined in 49 sites, distributed along all considered profiles with a spacing of 900 m. The corresponding RSR versus frequency curves have been classified using a logical-combinatorial algorithm. The results of the classification, in combination with the uppermost geological setting (geotechnical information and geological geometry of the subsoil) are used for the seismic microzoning of the city. Three different main zones are identified, and a small sector characterised by big resonance effects, due to the particular structural conditions. Each zone is characterized in terms of its expected ground motion parameters for the most probable strong earthquake ($M_S = 7$), and for the maximum possible ($M_S = 8$).

Introduction

In a previous paper, the realistic modelling of P-SV and SH waves for a frequency up to 1 Hz. was done for two profiles in Santiago de Cuba city (Alvarez et al., 2000). Those results show the influence of the basin structure on the ground motion, and indicate the limits and possibilities of using the modelling of waves propagation for microzoning purposes. In the framework of UNESCO/IUGS/IGCP 414 "Realistic modelling of seismic input for megacities and large urban areas", it has been decided to refine those results by using more detailed information about the shallow geology (geotechnical information, and geological geometry of the subsoil) and regional deep structure, and to extend them to all the present and perspective areas of the city. Santiago de Cuba is the second most populated city of Cuba. Located close to the boundary between Caribbean and North America plates, it is exposed to a relatively high level of seismic hazard (Alvarez et al., 1999, Rodríguez et al., 1997). Earthquakes felt in the city with I=VIII degrees on the MSK scale, have a recurrence period of about 80 years and there exists a high probability of occurrence of a $M_S = 7$ earthquake in the near future (Rubio, 1985) close to the city, in the Oriente transform fault system. This hypothetical earthquake is used as "scenario" for calculating synthetic seismograms along four profiles in the city by the hybrid technique (Fäh, 1992; Fäh et al., 1993, Fäh and Panza, 1994) based on modal summation and finite differences. The procedure computes wave trains generated by a seismic source buried in a regional crust-upper mantle structure (bedrock), and uses this motion as input to the local structure. The signals in the bedrock anelastic structure are generated by the modal summation approach (Panza, 1985; Panza and Suhadolc, 1987; Florsch et al., 1991; Panza et al., 2000); the waveforms along the local, laterally varying anelastic structure are then computed using a finite difference scheme (Virieux, 1984; 1986; Levander, 1988) applied to the local structure. The results of the modelling are used to make the seismic zoning of the local structure, using as microzoning criteria the "response spectra ratio" (RSR), i.e. the spectral amplification defined by { RSR = [Sa(2D)/Sa(1D)] }, where Sa(2D) is the response spectrum (at 5 % of damping) to the signals calculated for the laterally varying structure, and Sa(1D) is the one calculated for the signals in the bedrock structure.

Geological setting of Santiago de Cuba basin

Santiago de Cuba is characterised, from the geological point of view, by rocks, and stiff and unconsolidated sediments of different age, origin and lithological composition. The study region of the present work covers an area of approximately 250 Km^2. Recently, the analysis of new borehole data, as well as detailed field surveys, have supplied a more detailed geological map of Santiago de Cuba basin (Medina et al., 1999). Following those authors, three kinds of geological formations are present in the basin:

- Formations of the Paleogene Volcanic Arc. El Cobre Group is made up of several formations with a great complexity from the lithological point of view. It mainly consists of conglomerates and sandstones with tuffaceous composition, gravelites, tuffs, tuffites and limestones with lava flows of intermediate composition. They outcrop at the west and at the north of the study region and are presumed to be the bedrock fundament of the basin. This zone is not included in our study, because the development of the city is not oriented in that direction, due to its topographic characteristics.
- Neogene rocks. La Cruz formation is conformed of three members: Quintero, Tejar and Santiago. It is composed of polimitic conglomerates, calcarenites, argilites, calcareous sandstones, marls and reef sandstones, as well as of calcareous silts and sandy argilites. All members are represented in Santiago de Cuba city and its surroundings.
- Quaternary formations. They are of several kinds. The first one is mainly composed by gravelly alluvium (gravels, sands and clays with calcareous composition). We can find these soils mostly filling river basins, such as the San Juan River basin, in the eastern

part of the city. The second kind can be identified bounding the Santiago de Cuba and Cabañas bays, and is composed of sandy clays and peat, as well as man made ground and bay mud. Additionally are present the formations Camaroncito, Jaimanitas and Rio Maya, characterized by different kinds of limestone.

Three faults cross the basin (Arango, 1996; Pérez and García (1997). They are denominated El Cristo (present in the northwestern part of the study region), Bahía (along the east board of Santiago de Cuba Bay) and Sardinero (in the southeast corner of the study region).

A compilation of the structural parameters, geotechnical information, and geological geometry of the subsoil in Santiago de Cuba was constructed in the form of a database containing more than 600 boreholes' data. The quality of these data is variable and consists, in its majority, of visual description and classification of strata. The depth of penetration of boreholes varies: the majority reaches less than 25 m and only 3 reach approximately 200 m of depth.

Using these data, the generalized geological zoning has been performed compiling a set of maps representing the setting at different depths (5 m intervals close to the surface, 10-20 m intervals from 80 to 200 m). In the compilation of these maps, the real, very detailed lithological composition has been considered. The analysis of these maps, together with the consideration of the intervals of variation of the physical-mechanical properties of the rocks present in the geological maps, permitted us to simplify and generalize the map of Medina et al., (1999). The result of this generalization is shown in Fig 1. As can be seen from the figure, only 6 kinds of soils are present, corresponding to sands and sandstones of Quaternary formations, clays, sands and magmatic intrusions from Neogene formations, calcareous rocks and limestones from Neogene and Quaternary formations, as well as volcano-clastic rocks, tuffs, tuffites and agglomerates of El Cobre formation of the Paleogene Volcanic Arc. Additionally, significant lenses of gravely alluvium (gravels, sands and clays with calcareous composition) are present at depth in different parts of the basin.

Regional structural model

The crust structure in the region is very complicated, as can be seen in Alvarez et al., (2001) and we will use only a simplified regional model, consisting in a slight modification of the anelastic parameters of structure L of the cited paper (Fig. 2). This was constructed, for depth less than 30 Km, using the contribution of Arriaza (1998), who reinterpreted the results of Bobenko et al. (1980), while for depths ranging from 30 to 150 Km the results of the P waves tomography study of Van der Hilst (1990) and of the gravimetric study of Orihuela and Cuevas (1993) have been considered. For depths greater than 150 Km, the standard oceanic model of Harkrider (1970) is used.

The upper frequency limit for the numerical simulation has been fixed at 1 Hz. It means that our results are pertinent for ten and more storey buildings, lifelines, etc. This kind of building is present in Santiago de Cuba city, since approximately 15 years, when a program of construction of typical 12, 15 and 18-storey buildings began. A study of the microseisms spectral content, based on in situ measurements at the base and at the last floor of the buildings shows that free oscillation periods of 18-storey buildings are in the range 0.8-1.2 seconds (González, 1998; Seo et al., 1998). These periods tend to increase with the ageing of the building.

Two dimensional structural profiles in the basin

For studying the influence of the sedimentary basin structure on the seismic input, four profiles were selected across the basin. They follow the conditions that all the zones present in the simplified geological scheme of Fig. 1 are sampled (only the small bodies of magmatic intrusions were not included) and that the traces pass close to the places where the deeper boreholes of our database, are located. The corresponding cross sections have been prepared using, for depth < 50 m, mainly boreholes' data from a band, 0.25 Km wide at both sides of each

profile trace. More distant boreholes have been used for larger depths, up to 210 m. The cross sections show smooth transitions through the different zones and sharp ones when crossing the fault present in the study area. The data about the mechanical properties (P- and S-waves velocities and quality factors) of the strata (see Table 1) were taken from the literature (Pavlov, 1984, Ishihara, 1993, Berge-Thierry et al., 1999), as no direct measurements are available. The density is supported by laboratory measurements data, present in our database. The grid used in the finite differences calculations was selected with dimension, at the surface, $\Delta x = \Delta z = 0.015$ Km, in agreement with the details given in the sections.
The sources are placed on the Oriente transform fault system, at 30 Km of depth, and at a distance of 25 Km from the coast, in the main seismogenetic zone that affects the region, where the expected strong earthquakes are likely to be located. In Fig. 3 the locations of sources and the profiles traces are shown.

Results

a) Synthetic seismograms

Synthetic seismograms for SH-waves have been calculated along the selected profiles in the city by the hybrid approach (Fäh, 1992, Fäh et al., 1993). The sites are placed, on the surface, with a fixed spacing of 900 m. For each site we calculate displacement, velocity and acceleration seismograms for a point source with seismic moment $Mo = 1.0 \times 10^{13}$ N-m, focal depth $h = 30$ Km, and focal mechanism: dip = 21°, azimuth = 302° and rake = 21°. This mechanism corresponds to the Harvard University determination of one local earthquake that can be considered representative of the seismic sources in this sector of the Oriente fault zone. These seismograms have been then scaled, in the frequency domain (Panza et al., 1996), for possible earthquakes of different magnitude by using the scaling law of Gusev (1983), as reported by Aki (1987).
In Fig.4 the plots of the response spectra ratio, RSR, as functions of frequency and position along the profiles, are shown together with the corresponding cross sections. The RSR is larger and more variable, for frequencies greater than 0.4 Hz. At the end of profile 2 a clear resonance effect, characterized by very high values, that correspond, in the time domain to long wave trains is present. Additionally, it is clear the occurrence of two kinds of patterns. Those corresponding to profiles 2 and 3 are relatively smooth, in accordance with the smooth variation of the layering, while the ones corresponding to profiles 1 and 4 present rapid variations that are well correlated with the sharp lateral boundaries in the layers, due to the presence of a fault.

b) RSR curves classification

The RSR vs. frequency curves have been analysed in order to make the zoning of the basin. The RSR data for each site are sampled at 0.05 Hz from 0.39 to 0.99 Hz for a total of 13 points at each site. The obtained 49 curves are shown in Fig. 5. These data are processed, for the classification in compact sets, with a non-supervised logical-combinatorial algorithm included in PROGNOSIS system (Ruiz et al., 1992). To perform this analysis the curves are numbered continuously from the first (profile 1) to the last (profile 4), and in each profile from the beginning to the end. The main features of the algorithm are:

- Let the curve number "j" be the object "O_j", and the value of the RSR at frequency number "i" be the variable "x_i". Then, the value of RSR at the frequency number "i" in the curve number "j" will be "$x_i(O_j)$".
- Let $max(x_i)$ and $min(x_i)$ be the extremes of the variable x_i over all the objects. The similarity between objects is calculated by the formula

$$S(O_l, O_k) = 1/n \sum_{i=1}^{n} \frac{|x_i(O_l) - x_i(O_k)|}{\max(x_i) - \min(x_i)}$$

- Two objects O_i and O_j are β_o - *similar*, if and only if $S(O_i,O_j) \geq \beta_o$, where β_o is between 0 and 1. An object belongs to a compact set if the most similar to it is into this set too, or if it is the most similar to other object belonging to the set.
- The compact sets are graphically represented in a dendrogram, where the different β_o levels, in which they are grouped, can be seen. Selecting interactively, over this scheme, the level β_o, a particular partition in β_o - compact sets can be determined (Pico, 1999).
- The procedure starts determining the main β_o - compact sets; then, some of the sets can be subdivided using additional criteria, and the average curve for each final set is calculated.

Initially, for a level of similarity $\beta_o = 0.25$, 9 sets have been obtained. The first one, which comprised many curves with the smaller RSR values present in the data set, that form a wide sector in RSR vs. frequency graph, was subdivided in 4 subgroups attending to the range of variation, in average, of RSR. As a result 12 groups have been identified and their average curves are shown in Fig. 6.

In this set, 5 limit groups can be isolated. The curves 3, 6, 7 and 8 correspond to the last 4 sites in profile 2, where the surface waves resonance effect was identified, while curve 10 corresponds to the first sites in each profile, where no RSR increments can be expected. In Fig. 7 the results of classification are compared with the geological scheme of the basin. For the seismic zoning, a sort of correspondence between surface geology and RSR level was sought. After grouping several RSR levels into a common one; three such groups were identified: high - (2, 5, 9), intermediate - (4, 12), low - (1, 10, 11). Consequently, the microzoning of the basin was made in terms of these three groups. The boundaries between zones follow, whenever possible, the boundaries between the different elements of the geological map (slightly smoothed). For the zones not crossed by the profiles we took into account the results obtained in similar (by structure in depth) zones crossed by them. The microzoning scheme is shown in Fig. 8, where the small sub-zone, corresponding to the sites where the resonance effect has been identified, is delimited by a thick dashed line. The average RSR curves for each zone are shown in Fig. 9.

c) Expected Ground Motions

For getting information about the expected ground motions in the Santiago de Cuba basin, the obtained synthetic signals have been scaled to $M_S = 7$, the most probable strong earthquake, and to $M_S = 8$, the maximum possible earthquake, as estimated from seismotectonic considerations (Cotilla and Alvarez, 1991). From these scaled signals it has been determined the maximum ground motion displacement (d_{max}), velocity (v_{max}) and acceleration (a_{max}). As the frequency content of our signals is out of the range in which the maximum peak values of acceleration are commonly observed, the values of the design ground acceleration (DGA) are obtained by scaling acceleration seismograms with the design response spectra for the soils S1, S2 and S3 of the Cuban building code (Norma Cubana, 1999). A rough estimation of the real peak ground acceleration can be obtained from the maximum spectral value – MSV, through MSV = 2.5*DGA. A discussion of this procedure can be found in Panza et al. (1996) and Alvarez et al. (1999). In Tables 2 and 3 the results for $M_S = 7$ and $M_S = 8$ earthquakes, are reported respectively. Finally, recalling that the Effective Peak Acceleration (EPA) is defined as the average spectral acceleration in the period interval from 0.1 s to 0.5 s divided by 2.5 (Applied Technology Council, 1978), we see that EPA is equivalent to the DGA, calculated using design response spectra.

Discussion

The RSR patterns show the influence of the different geological features. There is a "regular" behaviour, characterised by very small RSR values, at small frequencies, followed by a smooth monotonous RSR increment from about 0.4 Hz, until 0.9 Hz, where the relative maximum is

reached, and a small decrease until 1 Hz. There are two exceptions to this relatively simple pattern. The first is at the end of profile 2, where the RSR pattern shows the appearance of very large amplitudes in the range 0.6 - 0.8 Hz, in the form of a narrow peak, followed by a sharp decrease towards 1Hz. In this part there is a thick clay layer, but before reaching it the waves travel through a structure where a relatively big lens of sand, of the small San Juan river basin, is embedded into the clays. It results in a cumulative increase of waves amplitude and duration, which remain after the sand lens is passed. This effect is similar to what has been obtained by Alvarez et al. (2001), where the largest RSR values for SH waves, along the San Juan river, were obtained at the sites where the thickness of Quaternary sediments was bigger. The second exception is represented by the oscillating RSR patterns, in the whole analysed frequency range, for the profiles 1 and 4, due to the presence of Bahía fault.
Our microzoning results are a scheme, not a map, because the density of RSR calculations is not sufficient to construct a map. Fig. 8 has been obtained extending our local results to the whole study area. Surface geology alone can't explain the different RSR patterns found and it is necessary to consider the data about the deeper structure. For example, the limestones in the south of the study region are classified in two different levels: to the west of San Juan River in the intermediate level, while to the east in the low level. This difference is due to the structure at depth; limestones in the west lie over marls, while in the east this layer of marls does not appear.

Conclusions

We study, along four profiles crossing Santiago de Cuba basin, the influence of the local soil conditions on seismic ground motion (SH-waves) due to earthquakes which occurred in the Oriente fault zone. A seismic microzoning of the city has been done considering (1) the synthetic response spectra ratios (RSR) computed at sites along these profiles, (2) the surface geology and (3) the deeper structure the basin. With the exception of four sites, where a big resonance effect, due to particular structural conditions, is present, all the RSR curves versus frequency have a common shape and differ only by their absolute value. Three different zones are identified. Each zone is characterized in terms of its expected ground motion parameters for two scenario earthquakes: the most probable ($M_S = 7$), and the maximum possible ($M_S = 8$). Where comparable, our results follow the general trend evidenced by previous investigations.

Acknowledgements

We acknowledge the support by MURST Cofin 2000 Project (Active Deformation at the Northern Boundary of Adria), CNR-C007F8_008, PNRA-Projects 1B and 3A and by the Associateship Program of the Abdus Salam International Centre for Theoretical Physics. This work is a contribution to the UNESCO-IUGS-IGCP Project 414 "Realistic Modeling of Seismic Input for Megacities and Large Urban Areas".

Bibliography

Alvarez, L., Romanelli, F. and Panza, G.F. (2001), *Synthetic seismograms in laterally heterogeneous anelastic media: Modal summation for the case of offshore seismic sources (deep-sea trough)*, The Abdus Salam ICTP Preprint IC/2001/169, 24 pp..

Alvarez, L., Vaccari, F., Panza, G.F. and González, B.E. (2001), *Modelling of ground motion in Santiago de Cuba City from earthquakes in Oriente fault seismic zone.* Pure appl. geophys., 158, pp. 1763-1782.

Alvarez, L., Vaccari, F., and Panza, G.F. (1999), *Deterministic seismic zoning of eastern Cuba*, Pure appl. geophys., 156, 469-486.

Applied Technology Council (1978) Tentative Provisions for the Development of Seismic Regulations for Buildings, U.S. National Bureau of Standards, Special Publication 510.

Arango, E. (1996), *Geodinámica de la región de Santiago de Cuba en el límite de las Placas de Norteamérica y el Caribe.* Tesis en opción al Grado de Master en Ciencias. Instituto Politécnico Nacional, México, D.F. 111pp.

Arriaza, G. (1998), *Nuevos enfoques en la interpretación y procesamiento de las ondas refractadas para el estudio del basamento de Cuba*, Tesis presentada en opción al grado científico de Doctor en Ciencias Geológicas, La Habana, 179 pp.

Aki, K, *Strong motion seismology*. In: *Strong Ground Motion Seismology*, NATO ASI Series, Series C: Mathematical and Physical Sciences, vol. 204, ed. Erdik, M.Ö and Toksöz, M. N. (D. Reidel Publishing Company, Dordrecht, 1987) pp.3-41.

Berge-Thierry, C., Lussou, P., Hernández, B., Cotton and E., Gariel, J.C. (1999), *Computation of the strong motions during the 19995 Hyogoken-Nambu earthquake, combining the k-square spectral source model and the discrete wavenumber technique.* In: *Proceedings of the Second International Symposium on the Effects of Surface Geology on Seismic Motion, Yokohama, Japan, 1-3 December, 1998; Volume 3, The Effects of Surface Geology on Seismic Motion, Recent Progress and New Horizon on ESG Study*, pp. 1414-1424.

Bovenko, V.G., Shcherbakova, B.Ye. and Hernández, G. (1980), *New geophysical data on the deep structure of eastern Cuba (in Russian)*, Sov. Geol., 9, 101-109.

Cotilla, M. and Alvarez, L. (1991), *Principios del mapa sismotectónico de Cuba*. Revista Geofísica del Instituto Panamericano de Geografía e Historia, No. 35, pp. 113-124.

Fäh, D. (1992), *A hybrid technique for the estimation of strong ground motion in sedimentary basins*, Ph.D. Thesis, Nr. 9767, Swiss Fed. Inst. Technology, Zurich, 161 pp.

Fäh, D., Iodice, C., Suhadolc, P. and Panza, G.F. (1993), *A new method for the realistic estimation of seismic ground motion in megacities, the case of Rome*, Earthquake Spectra, 9, 643-668.

Fäh, D. and Panza, G. F. (1994), Realistic modelling of observed seismic motion in complex sedimentary basins. Ann. Geofis., 37, 1771-1797.

Florsch, N., Fäh, D., Suhadolc, P. and Panza, G.F. (1991), *Complete synthetic seismograms for high-frequency multimode SH-waves*, Pure appl. geophys., 136, 529-560.

González, B.E. (1998), *El método de los microsismos en la solución de tarea de la sismología ingenieril*, Memorias del III Congreso cubano de Geología y Minería (GEOMIN98), Vol. I, pp. 284-286, Editorial Palcograf, ISSN 939-7117-01-0.

Gusev, A.A. (1983), *Descriptive statistical model of earthquake source radiation and its application to an estimation of short period strong motion*, Geophys. J. Roy. Astron. Soc., 74, 787-800.

Harkrider, D.G. (1970), *Surface waves in multilayered elastic media. Part II. Higher mode spectra and spectral ratios from point sources in plane layered Earth models*, Bull. Seism. Soc. Am., vol. 60, No. 6, pp. 1937-1987.

Ishihara, K., chairman (1993), *The Technical Committee for earthquake Geotechnical Engineering (TC-4) of the International Society for Soil Mechanics and Foundation Engineering, Manual for Zonation on Seismic Geotechnical Hazards,* The Japanese Society of Soil Mechanics and Foundation Engineering, 145 pp.

Levander, A.R. (1988), *Fourth-order finite-difference P-SV seismograms*, Geophysics, 53, 1425-1436.

Medina, A., Escobar, E., Ortíz, G. Ramírez, M., Díaz, L., Móndelo, F., Montejo, N., Diéguez, H., Guevara, T and Acosta, J. (1999), *Reconocimiento geólogo - geofísico de la cuenca de*

Santiago de Cuba, con fines de riesgo sísmico. Empresa Geominera de Oriente, Santiago de Cuba, 32 pp., graphic annexes.

Norma Cubana (1999), *Propuesta de nueva norma cubana sismorresistente*, 110 pp., (Draft).

Orihuela, N. and Cuevas, J. L. (1993), *Modelaje sismogravimétrico de perfiles regionales del Caribe central*, Revista Ingeniería, Universidad Central de Venezuela, 8, pp. 55-73.

Panza, G.F. (1985), *Synthetic seismograms: the Rayleigh waves modal summation,* J. Geophys. Res., 58, pp. 125-145.

Panza, G.F. and Suhadolc, P. (1987), *Complete strong motion synthetics.* In: B. A. Bolt (ed.) Seismic Strong Motion Synthetics, Computational Techniques 4, Academic Press, Orlando, 153-204.

Panza, G.F., Vaccari, F., Costa, G., Suhadolc, P. and Fäh, D. (1996), *Seismic input modelling for zoning and microzoning,* Earthquake Spectra, *12*, pp. 529-566.

Panza, G. F., Romanelli, F., and Vaccari, F. (2000), *Seismic wave propagation in laterally heterogeneous anelastic media: theory and applications to the seismic zonation, Advances in Geophysics*, Academic press 43, 1-95.

Pavlov O.Y., red. (1984), *Seismic microzoning* (in Russian), Moscow, Nauka.

Pérez, C. and García, D., *Tectónica de la Sierra Maestra (Sureste de Cuba).* In: *Estudios sobre Geología de Cuba*, ed. Furrazola, G. and Núñez, K (Centro Nacional de Información Geológica, Instituto de Geología y Paleontología, La Habana, 1997) pp. 462-473.

Pico, R. (1999), *Determinación del umbral de semejanza β_0 para los algoritmos de agrupamiento lógico-combinatorios, mediante el dendrograma de un algoritmo jerárquico.* SIARP'99, IV Simposio Iberoamericano de Reconocimiento de Patrones. Memorias, pp. 259-265

Rodríguez, M.; Alvarez, L. and García, J. (1997), *Estimaciones probabilísticas de la peligrosidad sísmica en Cuba.* Revista Geofísica del Instituto Panamericano de Geografía e Historia, No. 47, pp. 46-77.

Rubio, M. (1985), *The assessment of seismic hazard for the Republic of Cuba*, Ph.D. Thesis, Institute of Geophysics, Science Academy of Czechoslovakia, Prague.

Ruiz, J.; Pico, R.; López, R.; Alaminos, C.; Lazo, M.; Baggiano, M.; Barreto, E.; Santana, A.; Alvarez, L. and Chuy, T. (1992): *PROGNOSIS y sus aplicaciones a las geociencias.* In: IBERAMIA-92, III Congreso Iberoamericano de Inteligencia Artificial, MEMORIAS. México, LIMUSA, pp. 561-586.

Seo, K., González, B.E., Arango, E., et al. (1998), *Past, present and perspective research on seismic microzoning in the cities of Santiago de Cuba and Havana*, Proceedings of the workshop to exchange research information in the international scientific research project "Joints studies on seismic microzonation in earthquake countries", Tokyo Institute of Technology, Japan, 17 pp.

Van der Hilst, R. D. (1990), T*omography with P, PP and pP delay-time data and the three-dimensional mantle structure below the Caribbean region*, Ph.D. Thesis, University of Utrecht.

Virieux, J., 1984 - *SH-wave propagation in heterogeneous media: velocity-stress finite-difference method*, Geophysics, 49, 1933-1957.

Virieux, J.,1986 - *P-SV wave propagation in heterogeneous media: velocity-stress finite-difference method*, Geophysics, 51, 889-901.

No.	Brief Description	V_P	V_S	ρ	Q_P	Q_S
1	Sands	1.2	0.35	1.8	100	50
2	Clays	0.8	0.3	1.6	100	50
3	Marls	1.3	0.6	2.0	150	50
4	calcareous soils	0.9	0.5	1.8	150	50
5	Calcareous rocks	2.5	1.4	2.3	200	100
6	Igneous rocks	2.4	0.8	2.1	350	150

Table 1. Physical properties of the different layers present in the selected profiles

No.	d_{max}	v_{max}	a_{max}	DGA_{S1}	DGA_{S2}	DGA_{S3}
Profile 1, =103.9 Km to the beginning of profile						
1	0.23	0.09	0.22	0.74	0.43	0.36
2	0.24	0.13	0.41	1.65	1.12	0.97
3	0.24	0.12	0.39	1.36	0.92	0.80
4	0.24	0.10	0.30	0.99	0.66	0.55
5	0.24	0.11	0.25	0.82	0.55	0.48
6	0.24	0.11	0.28	1.18	0.80	0.70
7	0.24	0.11	0.34	1.46	0.99	0.86
8	0.24	0.10	0.34	1.23	0.83	0.72
9	0.24	0.09	0.28	0.77	0.53	0.46
10	0.23	0.09	0.25	0.76	0.45	0.36
11	0.23	0.09	0.24	0.76	0.45	0.36
12	0.23	0.09	0.22	0.74	0.46	0.39
13	0.23	0.09	0.21	0.74	0.49	0.42
14	0.24	0.10	0.27	0.96	0.64	0.54
Profile 2, =43.5 Km to the beginning of profile						
15	2.48	3.26	9.89	30.14	19.93	16.86
16	2.63	3.89	12.91	41.41	27.71	23.59
17	2.55	3.60	11.65	36.59	24.30	20.61
18	2.48	3.40	10.63	32.90	21.85	18.48
19	2.43	3.32	10.06	31.31	20.66	17.44
20	2.37	3.27	9.64	29.48	19.58	16.56
21	2.32	3.26	9.56	29.26	19.43	16.51
22	2.37	3.60	11.55	36.75	24.79	21.28
23	2.49	4.00	14.48	51.52	34.75	29.83
24	2.74	4.37	18.96	82.81	55.85	47.94
25	2.92	5.06	22.55	149.45	99.24	83.93
26	2.98	5.14	18.93	163.39	107.82	90.49
27	2.96	4.71	16.61	165.08	107.54	89.13
Profile 3, =34.5 Km to the beginning of profile						
28	3.12	3.76	11.94	36.29	24.10	20.38
29	3.31	4.54	15.78	50.88	34.28	29.43
30	3.21	4.23	14.48	44.54	29.81	25.38
31	3.14	4.14	13.73	41.67	27.67	23.55
32	3.07	4.07	12.88	39.27	26.08	22.06
33	3.01	4.12	12.76	38.97	25.97	22.11
34	2.96	4.15	12.71	39.46	26.41	22.48
35	2.97	4.32	13.87	44.58	29.83	25.52
36	2.98	4.47	14.78	47.74	31.95	27.35
37	3.08	4.91	17.47	57.49	38.47	32.83
38	3.02	4.79	16.66	54.92	36.75	31.29
39	3.18	5.48	20.30	70.65	47.28	40.25
Profile 4, =33.6 Km to the beginning of profile						
40	1.87	2.46	7.55	22.77	15.12	12.79
41	2.03	3.16	11.01	36.06	24.32	20.87
42	2.04	3.21	11.43	37.25	25.12	21.56
43	1.99	3.10	10.68	34.81	23.30	19.96
44	2.04	3.45	12.31	42.50	28.66	24.60
45	2.02	3.47	12.51	43.47	29.32	25.16
46	2.01	3.60	13.32	47.12	31.78	27.28
47	1.98	3.68	13.82	49.87	33.64	28.87
48	1.96	3.70	13.91	51.18	34.52	29.63
49	1.89	3.49	12.88	46.97	31.68	27.19

Table 2. Ground motion parameters for an earthquake of $M_S = 7$ in the sites located along all the profiles.

No.	d_{max}	v_{max}	a_{max}	DGA_{S1}	DGA_{S2}	DGA_{S3}
Profile 1, _ = 103.9 Km to the beginning of profile						
1	1.62	0.55	0.94	3.20	1.88	1.58
2	1.62	0.71	1.86	7.56	5.14	4.45
3	1.62	0.66	1.79	6.24	4.24	3.67
4	1.60	0.59	1.29	4.48	2.96	2.48
5	1.58	0.61	1.15	3.69	2.51	2.17
6	1.58	0.62	1.28	5.41	3.68	3.19
7	1.58	0.60	1.51	6.63	4.51	3.91
8	1.58	0.57	1.55	5.62	3.82	3.31
9	1.57	0.51	1.29	3.55	2.42	2.09
10	1.57	0.50	1.13	3.14	1.96	1.62
11	1.56	0.50	1.06	3.19	1.97	1.61
12	1.56	0.50	0.99	3.12	2.05	1.73
13	1.56	0.48	0.96	3.33	2.21	1.87
14	1.57	0.49	1.20	4.31	2.86	2.42
Profile 2, _ = 43.5 Km to the beginning of profile						
15	15.92	14.84	44.33	135.40	89.91	76.14
16	16.50	17.64	58.11	188.10	125.88	107.17
17	16.08	16.28	52.36	165.11	109.93	93.59
18	15.67	15.39	47.52	148.42	98.55	83.36
19	15.39	15.00	44.77	140.42	93.24	78.86
20	15.05	14.88	42.91	133.23	88.47	74.99
21	14.80	14.83	42.97	131.95	88.04	74.96
22	14.97	16.29	52.27	167.51	112.98	96.97
23	15.48	18.04	65.33	237.10	159.92	137.26
24	16.55	19.87	85.05	381.56	257.35	220.89
25	17.25	22.34	1.60	673.84	447.48	380.98
26	17.59	21.59	85.68	720.94	475.74	399.28
27	17.19	21.31	76.39	726.95	473.54	392.50
Profile 3, = 34.5 Km to the beginning of profile						
28	16.49	16.92	53.16	164.03	108.92	92.58
29	17.26	20.39	70.54	232.10	156.54	134.37
30	16.78	19.04	65.10	202.42	135.46	115.33
31	16.40	18.66	61.83	188.02	125.57	106.91
32	16.00	18.38	57.89	177.08	117.59	100.01
33	15.68	18.61	57.27	176.34	118.01	100.47
34	15.37	18.72	56.81	179.56	120.17	102.31
35	15.33	19.45	61.94	203.08	135.90	116.61
36	15.32	20.09	66.17	217.45	145.58	124.95
37	15.71	22.11	78.71	262.27	175.51	150.25
38	15.38	21.57	74.95	250.37	167.55	142.65
39	16.00	24.71	91.45	322.09	215.55	183.51
Profile 4, = 33.6 Km to the beginning of profile						
40	9.84	11.09	33.72	102.82	68.27	58.06
41	10.49	14.26	49.85	164.17	110.72	95.04
42	10.48	14.54	51.72	170.12	114.40	98.20
43	10.17	14.02	47.76	158.69	106.23	91.18
44	10.36	15.63	54.62	194.82	131.40	112.79
45	10.20	15.62	55.95	198.92	134.16	115.16
46	10.12	16.09	59.97	215.44	145.31	124.72
47	9.99	16.63	62.95	229.12	154.53	132.64
48	9.82	16.82	63.29	234.00	157.82	135.46
49	9.46	15.87	57.98	214.77	144.86	124.34

Table 3. Ground motion parameters for an earthquake of $M_S = 8$ in the sites located along all the profiles.

Figure captions

Fig. 1. a) Simplified geological scheme of Santiago de Cuba basin (modified from Medina et al., 1999), 1 - sand and sandstones (Quaternary formations), 2 - clays (Neogene), 3 - marls (Neogene), 4 - magmatic intrusions, 5 - calcareous rocks and limestones (Neogene and Quaternary formations), 6 - rocks from El Cobre formation (Paleogene Volcanic Arc), 7 - faults; the ticks on the frame of the figure are 1 K m apart, the left-low corner has coordinates 19.954° N and 75.897° W.

Fig. 2. a) Regional structural model; b) Detail of the first 40 Km.

Fig. 3. a) Position of the sources and profiles; b) Detail of profiles traces in the basin and city plan (filled by points are human settlements, filled by crossing lines are industrial areas); The ticks on the frame of the figure are 1 K m apart, the left-low corner has coordinates 19.945° N and 75.945° W.

Fig. 4. Relative response spectra (RSR) of SH waves as a function of frequency along each profile. The models of each profiles are plotted below each panel. The numbers along the x-axes correspond to the ordinal site position., The numbering in the legend corresponds to the different layers, whose parameters are given in Table 1.

Fig. 5. Response spectra curves for all profiles from 0.39 to 0.99 Hz, sampled at 0.05 Hz.

Fig. 6. Typical RSR curves versus frequency obtained as a result of the classification procedure. a) All the groups; b) Detail after removing the four curves that present anomalous higher values.

Fig. 7. Representation of the results of the classification of all curves over the geological map. The numbers correspond to the typical curves shown in Fig. 6, while the legend is equivalent to the corresponding of Fig. 1. The ticks on the frame of the figure are 1 K m apart, the left-low corner has coordinates 19.954° N and 75.897° W.

Fig. 8. Microzoning of Santiago de Cuba basin: 1 - low RSR level, 2 - intermediate RSR level, 3 - high RSR level, 4 - subzone, of the previous one, where resonance effect was identified, 5 - zone of El Cobre formation, not included in our analysis, 6 - San Juan river. The ticks on the frame of the figure are 1 K m apart, the left-low corner has coordinates 19.945° N and 75.945° W.

Fig. 9. Average RSR curves versus frequency for each zone of the microzoning scheme: 1 - low RSR level, 2 - intermediate RSR level, 4 - high RSR level.

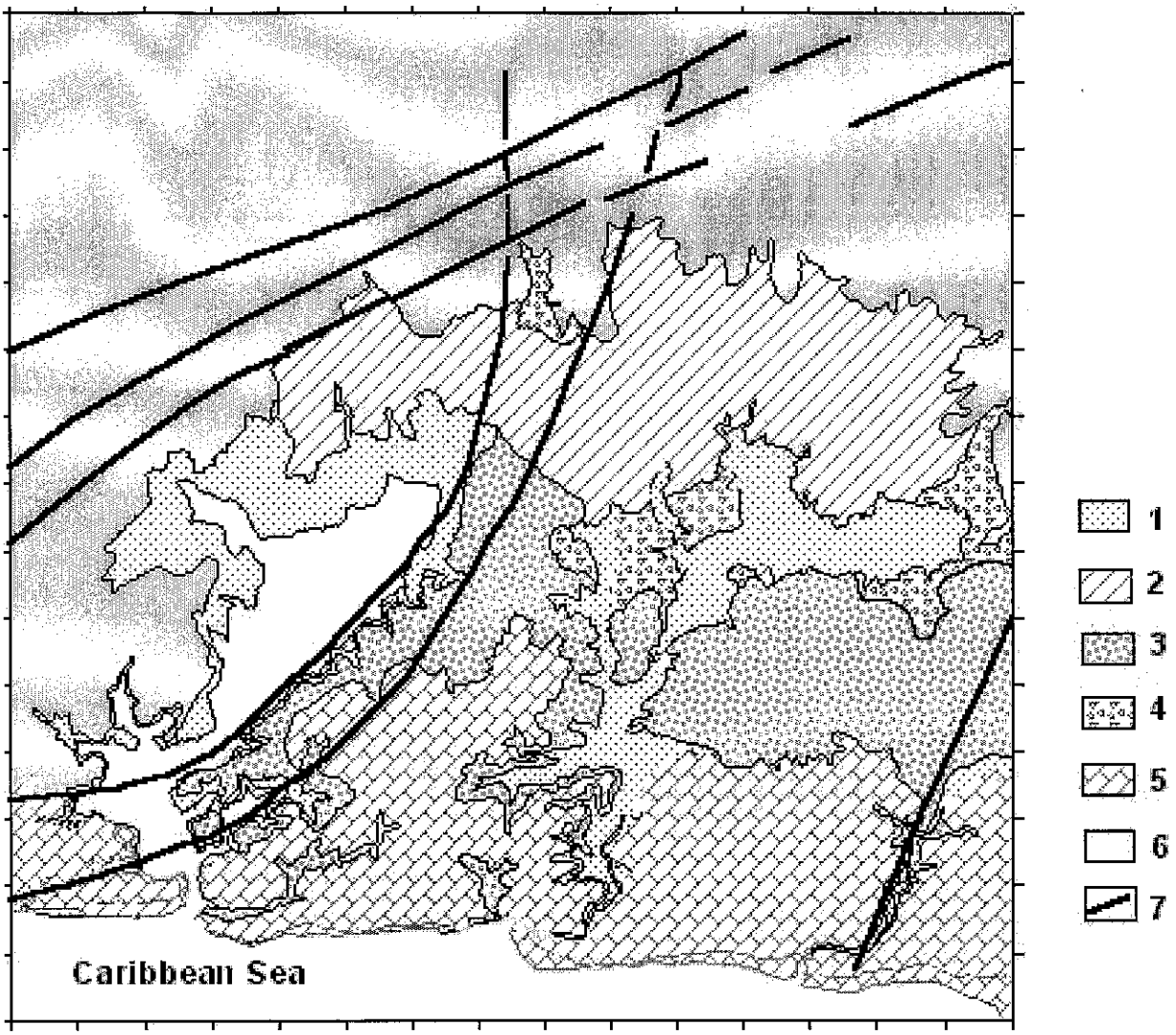

Figure 1

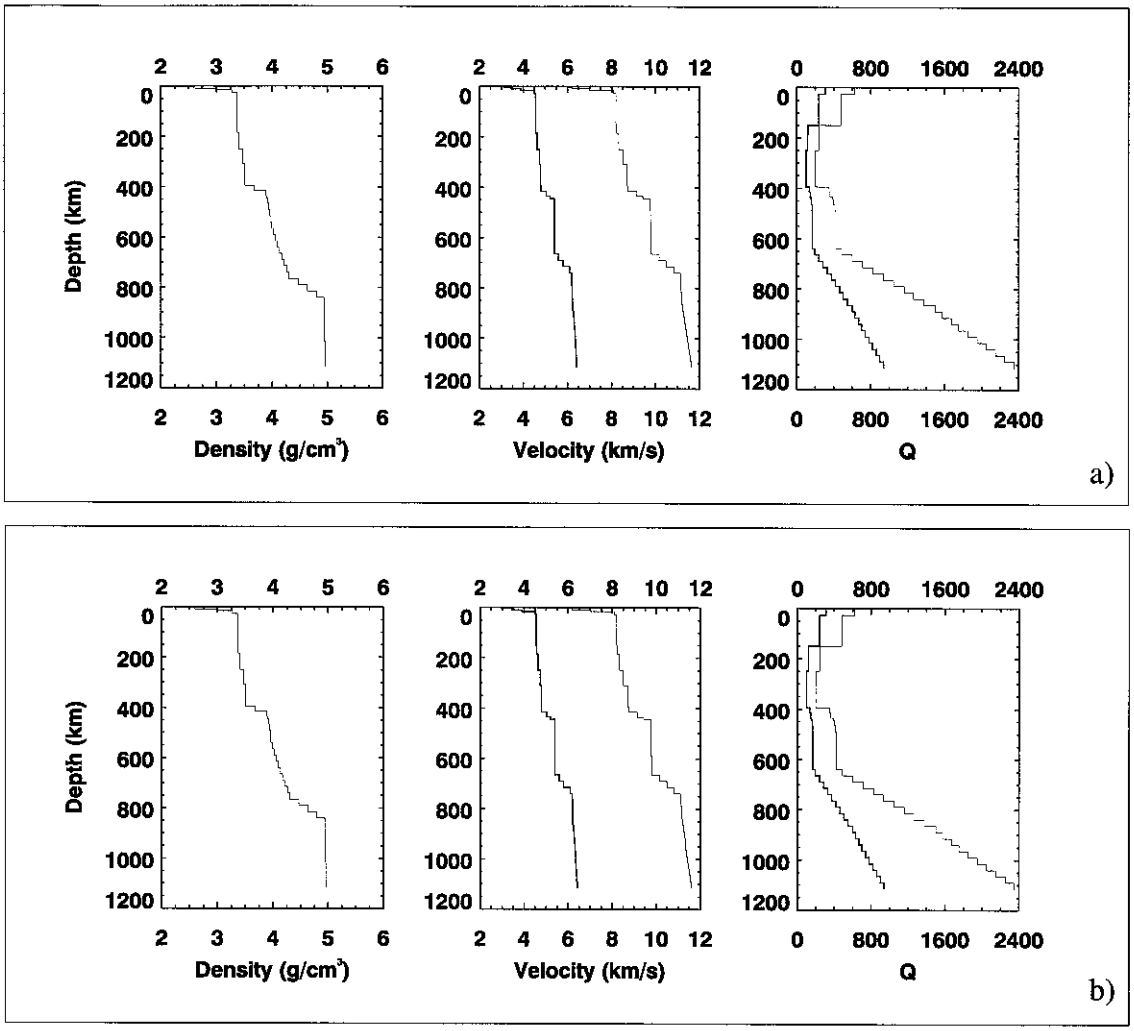

Figure 2

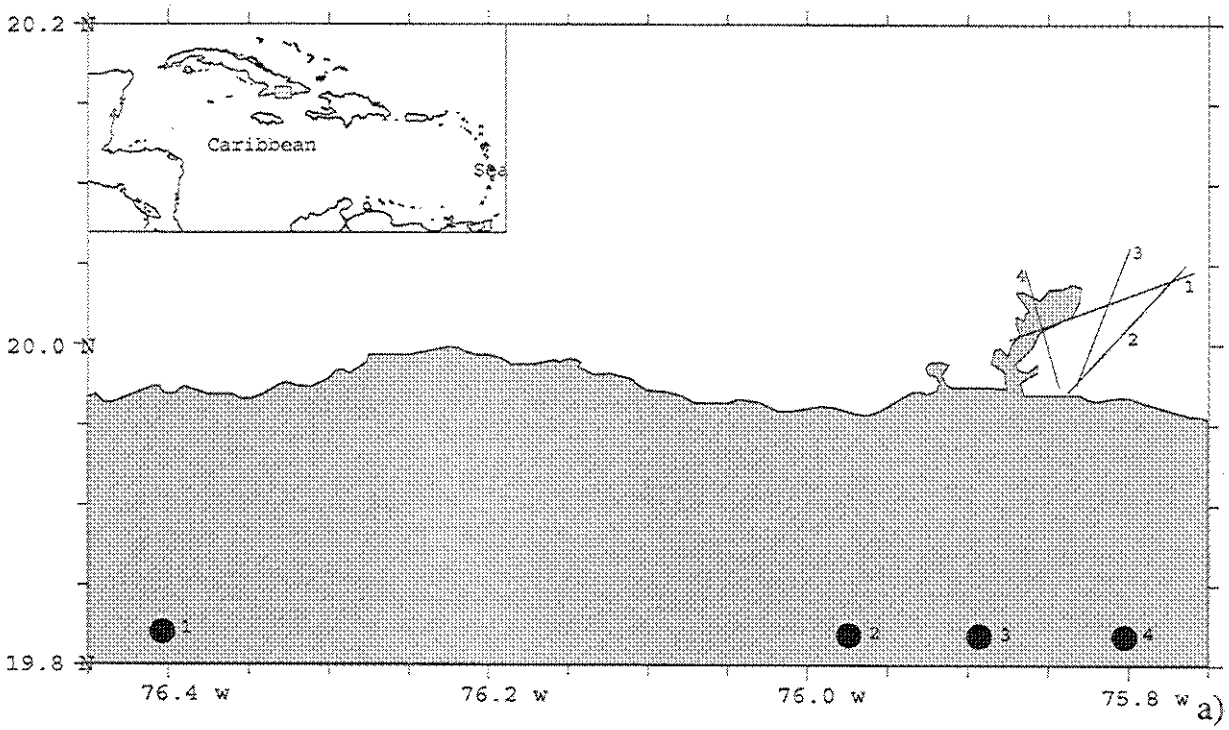
20.2 N
20.0 N
19.8 N
Caribbean
Sea
1
2
3
4
76.4 w
76.2 w
76.0 w
75.8 w
a)

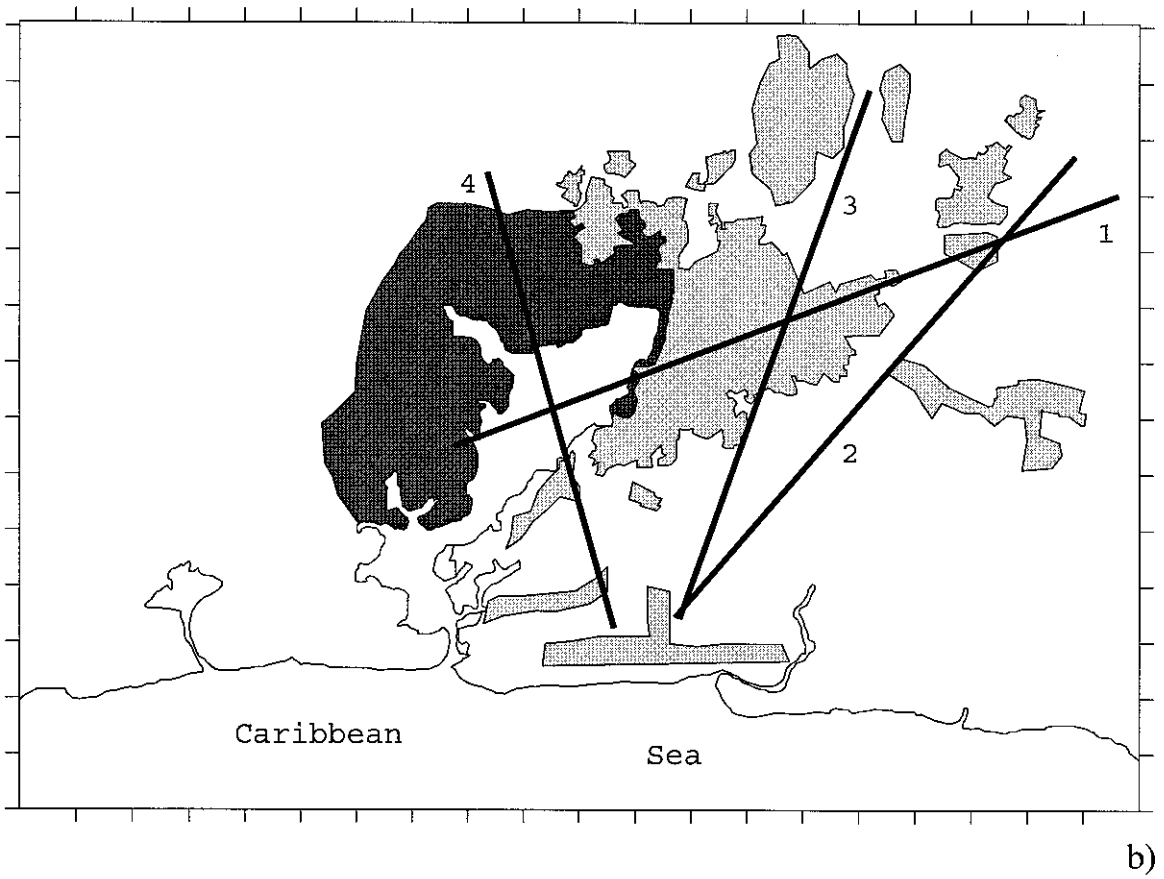
4
3
1
2
Caribbean
Sea
b)

Figure 3

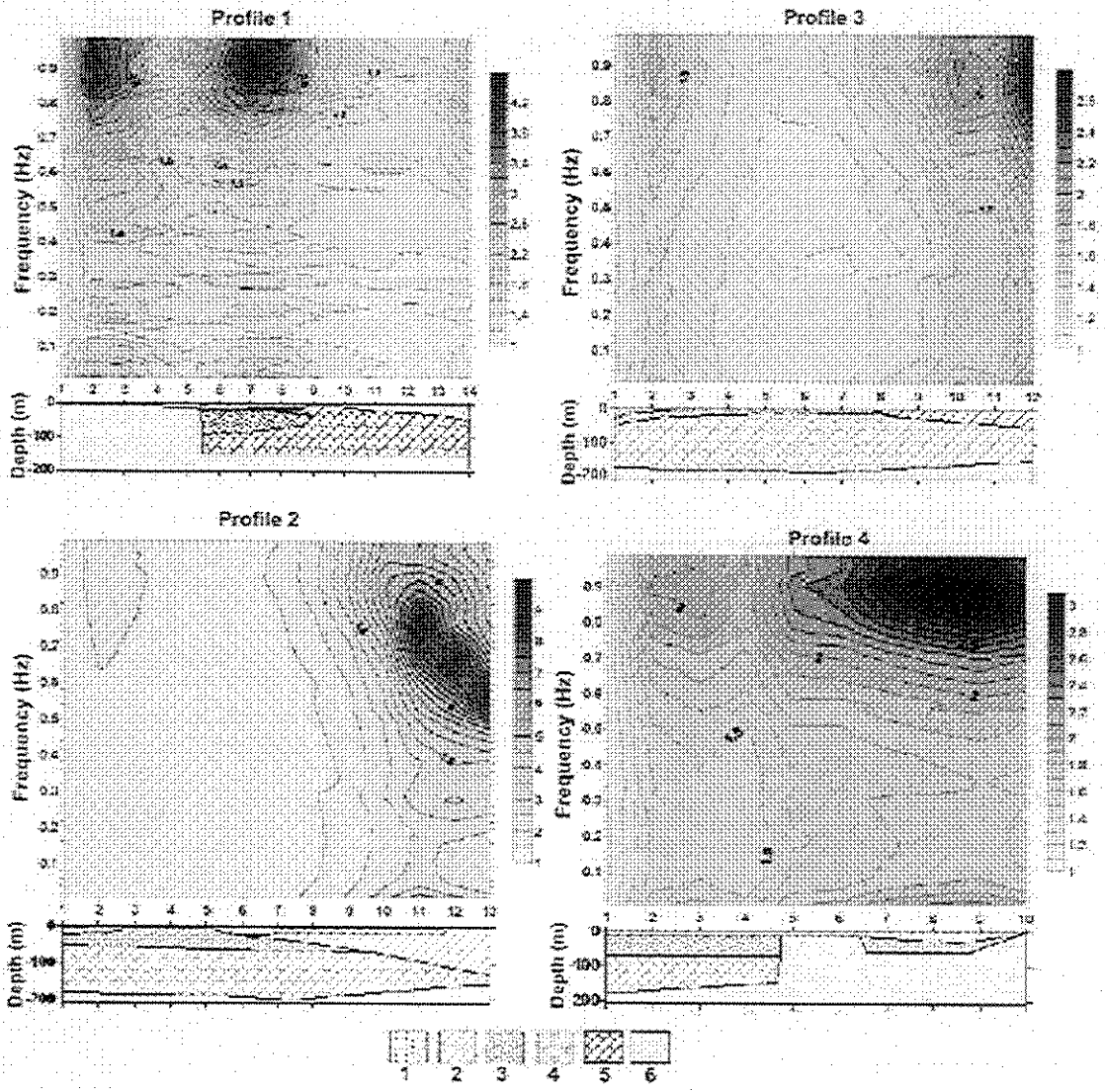
Profile 1
Profile 3
Profile 2
Profile 4
Frequency (Hz)
Depth (m)
1
2
3
4
5
6

Figure 4

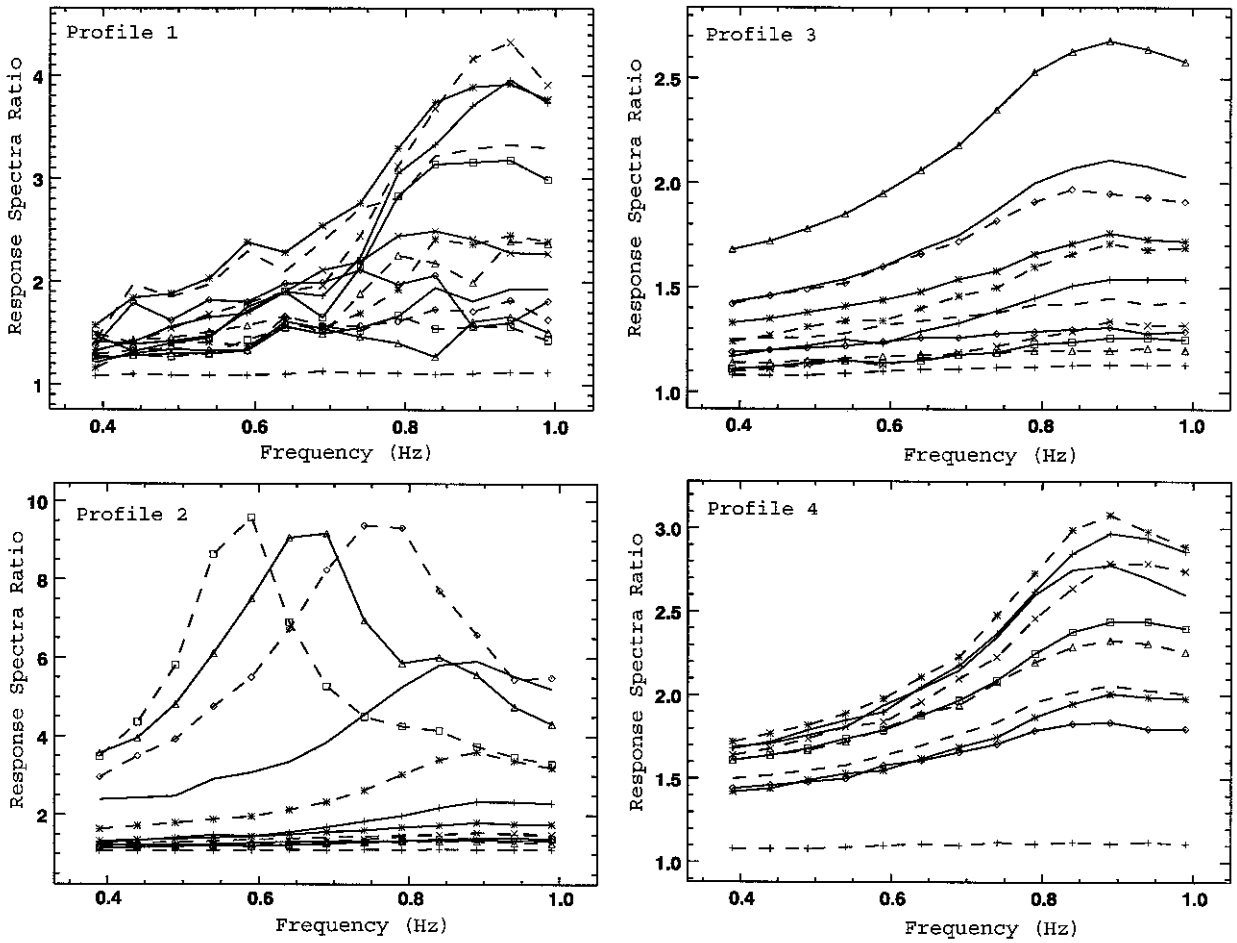
Profile 1
Response Spectra Ratio
Frequency (Hz)
Profile 3
Response Spectra Ratio
Frequency (Hz)
Profile 2
Response Spectra Ratio
Frequency (Hz)
Profile 4
Response Spectra Ratio
Frequency (Hz)

Figure 5

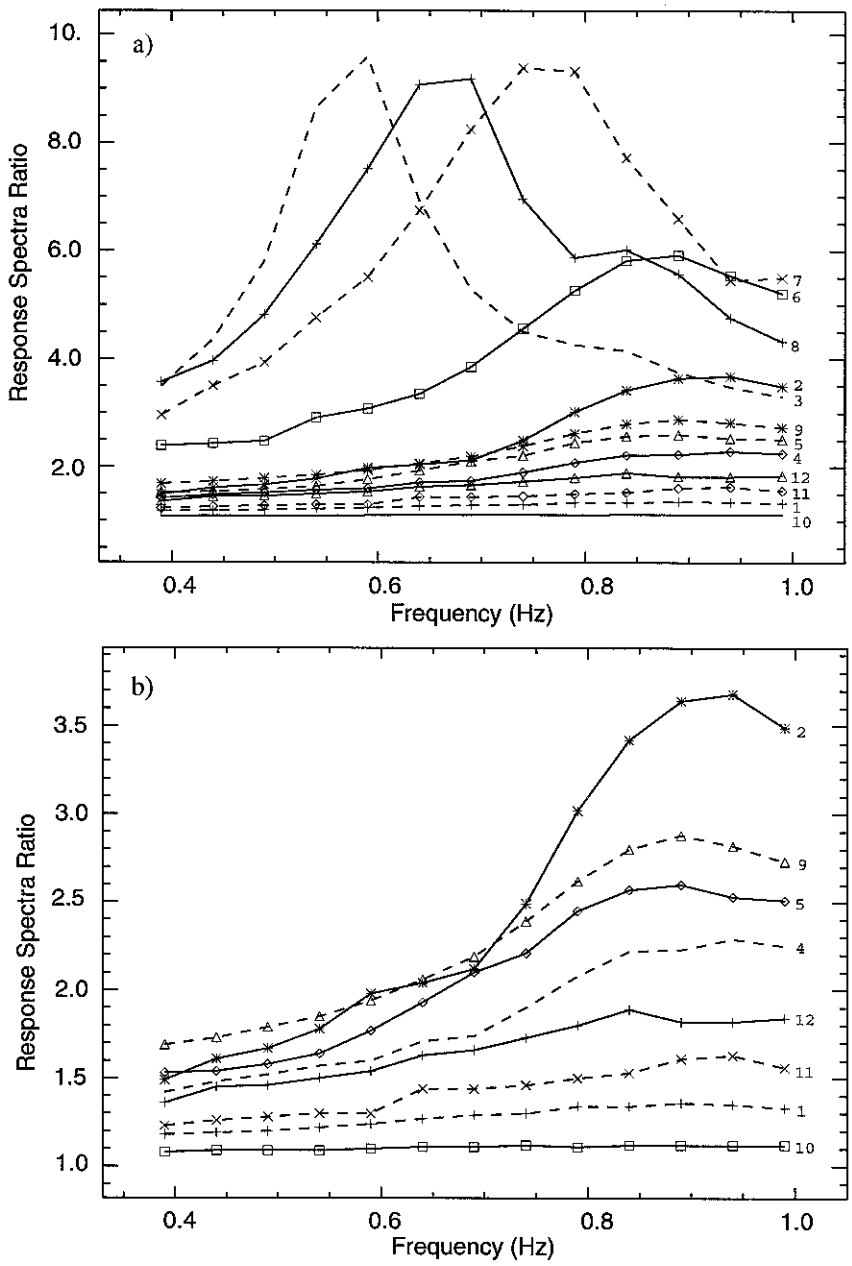
a)
Response Spectra Ratio
10.
8.0
6.0
4.0
2.0
0.4
0.6
0.8
1.0
Frequency (Hz)
7
6
8
2
3
9
5
4
12
11
1
10
b)
Response Spectra Ratio
3.5
3.0
2.5
2.0
1.5
1.0
0.4
0.6
0.8
1.0
Frequency (Hz)
2
9
5
4
12
11
1
10

Figure 6

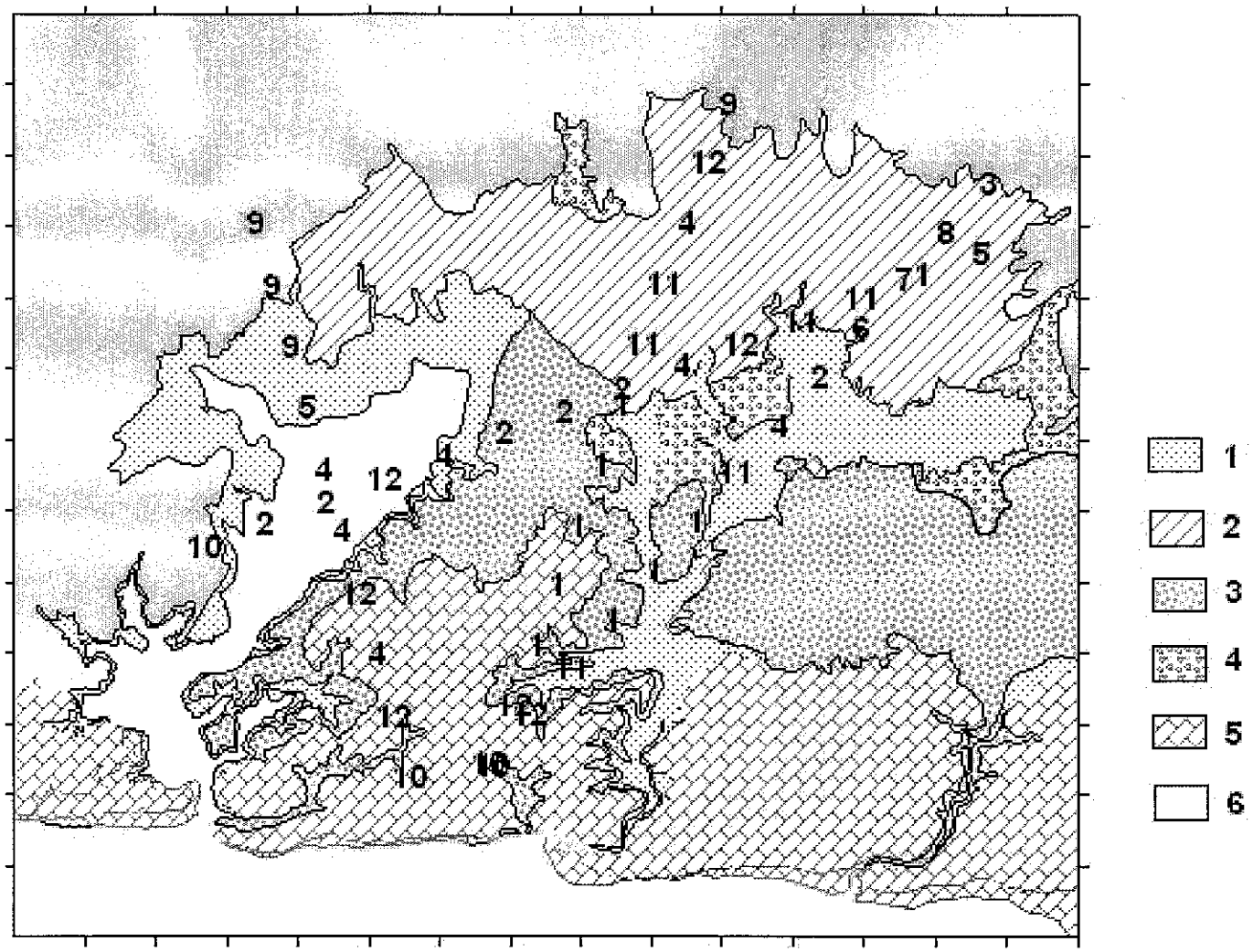

Figure 7

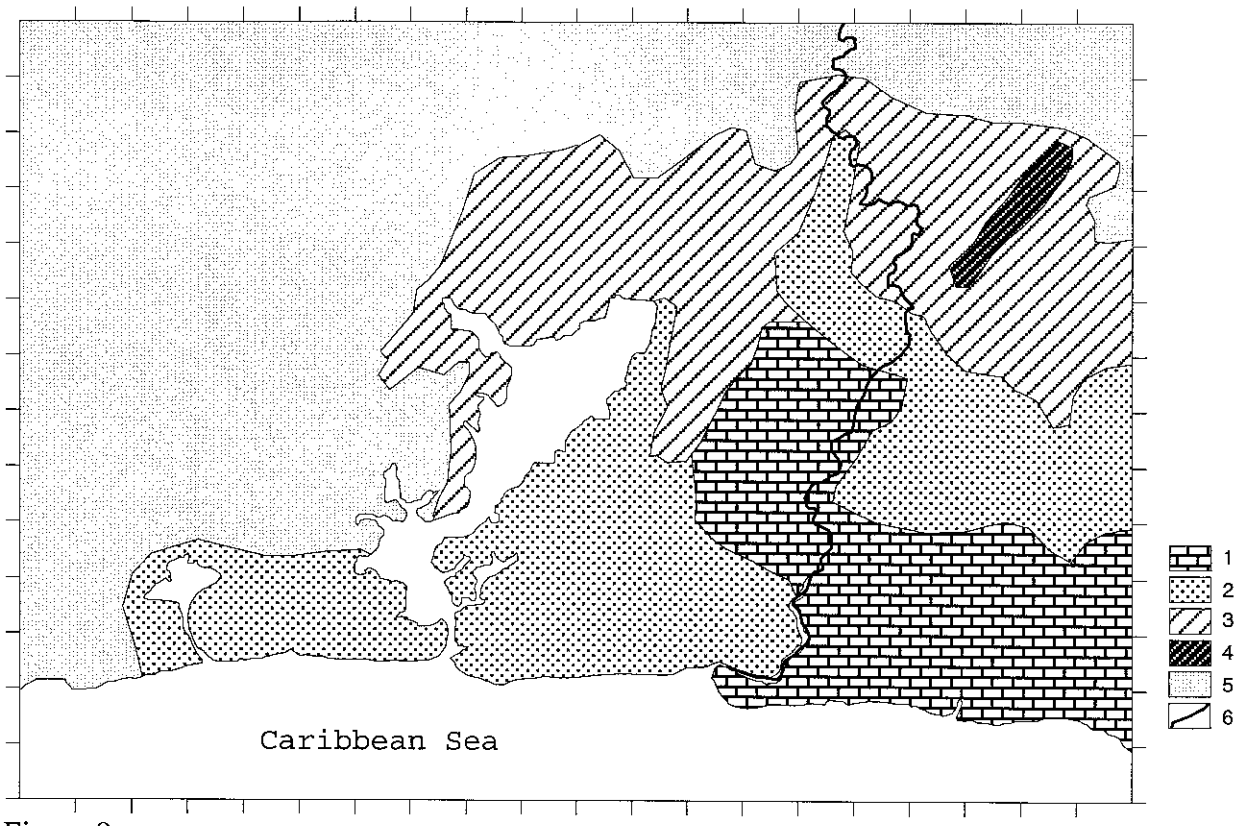

Figure 8

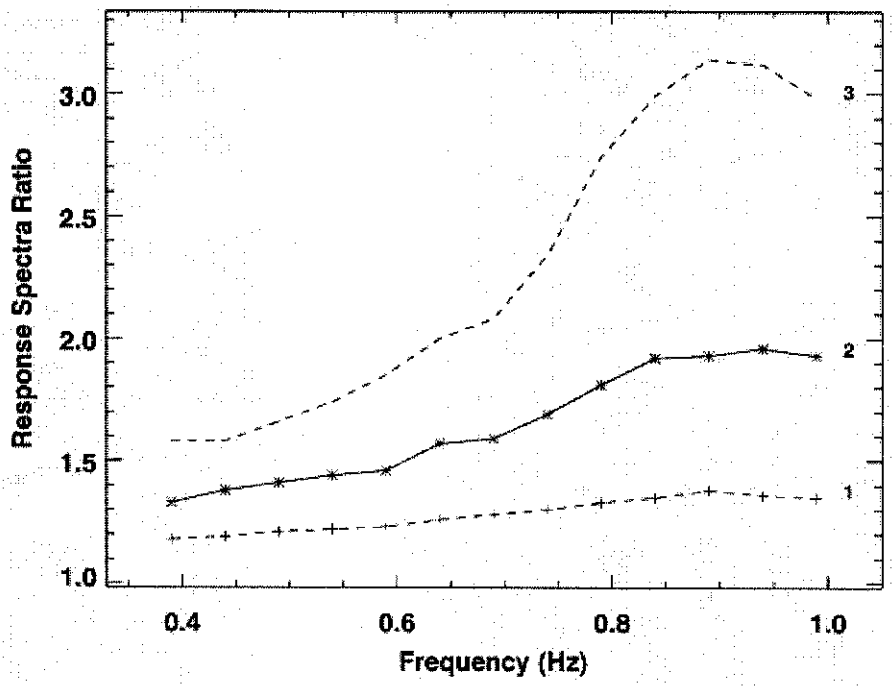
Response Spectra Ratio
3.0
2.5
2.0
1.5
1.0
0.4
0.6
0.8
1.0
Frequency (Hz)
3
2
1

Figure 9